Modelling Pollution Transport Dynamics and Mixing in Square Manhole Overflows

Modupe Jimoh[a*] and Soroush Abolfathi [a]

[a] School of Engineering, University of Warwick, Coventry, CV4 7AL

[*] Corresponding author's email: jimohmodupe1@gmail.com

co-author's email: Soroush.abolfathi@warwick.ac.uk

Modelling Pollution Transport Dynamics and Mixing in Square Manhole Overflows

Abstract

Detailed knowledge of the dynamic interactions between incoming sewerage and an overflowing manhole, and the resulting pollutant concentrations from manhole flooding, are critical for robust design and operations of wastewater infrastructures, especially during extreme climatic events. This study investigates the mixing and dispersion of solute in square manhole overflow using laboratory tracer experiment and analytical modelling. Tests are conducted with three flow rates to examine mixing characteristics over a wide range of operational conditions. Two overflowing scenarios including blocked pipe exit, and overflow in combination with pipe exit are studied. The Residence Time Distributions (RTD) and longitudinal dispersion coefficients are determined to understand the characteristics of pollutant transport. The analysis of the fluorometric tracer data show the appropriateness and robustness of the deconvolution model adopted in this study for determining the mixing characteristics and RTDs (R^2>0.95). Similarly, the Taylor's model was shown to be capable of predicting advective and dispersive mixing mechanisms within the manhole, for the range of flow conditions tested in this study. New empirical predictive formulae are derived to characterise the pollutant mixing in square manholes under different operational conditions.

Keywords: Overflow, Pollution transport, Residence Time Distribution, Square manholes Urban Flooding.

Highlights

- Hydraulic performance and solute dispersion in square manhole is investigated through fluorometric tracer tests.
- Mixing coefficient was determined and new predictive formulae were derived to inform modelling and design of square manholes.
- Overflow from manholes affect the surrounding environment and pose health hazards to the immediate community and ecosystems.

1.0 Introduction

Rapid increase in urban developments and the consequent impermeable floors has reduced the natural infiltration capacity in many developed regions (Strohbach et al., 2019). This has led to increased volume of rainwater entering the combined sewer systems and inadequate capacity of sewer networks during extreme climatic events (Feng, Zhang, & Bourke, 2021). This is a particularly important problem in the face of climate change (GebreEgziabher & Demissie, 2020), where increased intensity and frequency of extreme climatic events are expected in the coming decades (Miller & Hutchins, 2017). Flooding through manholes can be triggered by increased rainfall events, blockages, pumping station failure, defects in the sewerage network or surcharging in the downstream of combined sewers. The pollutant content in sewers generally contains; suspended solids, nutrients (nitrogen and phosphorus), dissolved minerals, organic matter (measured as biochemical oxygen demand or BOD), toxic contaminants (both organic and inorganic), and micro-organisms or pathogens which can cause disease (Von Sperling, 2007; O. Mark et al., 2018; Schreiber et al., 2019; Borzooei et al., 2020). The hydraulic performance of manholes is a complex function of the flow-sewer interactions influenced by incoming flow characteristics, manhole geometry, the ratio between sewer and manhole size, surface roughness and the surcharge features (Ole Mark & Ilesanmi-Jimoh, 2017). The wastewater transport in sewer system through advective and dispersive mixing mechanisms, resulting in temporal and spatial variations in the concentration of solute and solid pollutants in the sewer network, and the supporting hydraulic infrastructures (GebreEgziabher & Demissie, 2020). Hence, determining the dispersion processes in the sewer system is critical to understand when, and at what concentrations, pollutants arrive at downstream locations vulnerable to overflow and flooding.

Mathematical modelling and quantification of the underlying mechanisms which govern solute mixing can lead to the appropriate estimation of the spatial and temporal variations of the dispersion coefficient (D_{xx}) in water and wastewater transport systems (Goodarzi et al., 2020). Pioneering work by Taylor on pipe flow (Taylor, 1954), shows that, with plug flow assumptions, at some distance downstream of the tracer injection, an equilibrium becomes established between transverse shear velocity influencing longitudinal dispersion, and transverse diffusion which counteracts longitudinal dispersion (Rutherford, 1994). Taylor's dispersion conceptualises that the process of solute transports in flowing solvent combines the effects of molecular diffusion and transverse non-uniformity of vertical variation of velocity profiles (Abolfathi & Pearson, 2014, 2017; Wang & Chen, 2016). The solute transport processes within the flow can then be described by Taylor's Advection Dispersion Equation (ADE) as:

$$c(x,t) = \frac{M}{A\sqrt{4\pi D_{xx}t}} exp\left[-\frac{(x-ut)^2}{4D_{xx}t}\right] \quad (1)$$

where c (x, t) is the concentration of tracer at position x and at time t, A is the cross-sectional area of pipe [m^2], M denotes the mass of tracer [kg], u is the mean particle velocity derived from L/t_{rtd} [m/s], t_{rtd} is the mean residence time [s], L is the length between the tracer input and output point [m] and, D_{xx} is the longitudinal dispersion coefficient [m^2/s]. Given the non-circular shape and the width to length ratio of the manhole prototype used in this study, we adopt the mean particle velocity for the tracer analysis.

The pollution transport mechanisms between sewer and manholes can be modelled using a range of analysis methods. One of the well-established approaches to modelling solute transport within complex engineered flow systems is to consider the system's residence time distribution. RTD describes the hydraulic system's response to an instantaneous, i.e. pulse, upstream tracer injection (Guymer & Stovin, 2011). Sonnenwald et al. (2015) used the deconvolution algorithm to analyze pollution transport across a range of manhole and pipe configurations. Analysis of Sonnenwald et al. (2015) results shows correlation values between 0.983 to 0.998, indicating that the maximum entropy deconvolution method can robustly predict the mixing profiles.

Currently, the existing literature mainly focuses on understanding pollutant mixing within circular manhole geometries. Despite structural necessity and frequent usage of square manholes, there are still gaps of knowledge in understanding the pollution mixing dynamics and interactions between incoming wastewater and square manholes. This paper bridges this knowledge gap and provides a comprehensive understanding of mixing processes and pollution transport mechanisms within square manholes. The paper showcases the dynamics of pollution transport in overflowing square manholes by undertaking laboratory-scale physical modelling tests to determine the temporal variations of the tracer concentrations at points upstream, downstream, and overflow from the square manhole. The results evaluate the performance and pollution discharge risks of square manholes under a range of operating conditions including extreme climatic events.

2.0 Method

2.1 Manhole Configuration

The experimental setup, depicted in Figure 1, consists of a square manhole with a cross-sectional area of 150 mm × 150 mm and a height of 700 mm to create a manhole prototype with a width to pipe diameter ratio of 3.0. A pipe with internal diameter of 50 mm extends horizontally on both sides of the

manhole creating a straight-through flow, with the ends acting as inlet and outlet, respectively. The experimental setup is designed to represent a scaled-down version of the square manhole-pipe configuration recommended by water industry standards (Water-UK, 2019). The depth of water in the pipe is controlled with a sluice gate installed at the downstream end of the manhole physical modelling setup, enabling creation of different flood scenarios. The physical model is continuously fed with water recirculating around the system from a 4 m^3 sump. A weir was fitted around the top of the manhole with the surcharge height of 730 mm, enabling a steady overflow of water into a stilling basin. The stilling basin was made of Perspex with the dimensions of 570 mm by 500 mm and depth of 115 mm, collecting the overflowing water. In addition, the basin was fitted with a trough that conveys the water into the sump for recirculation.

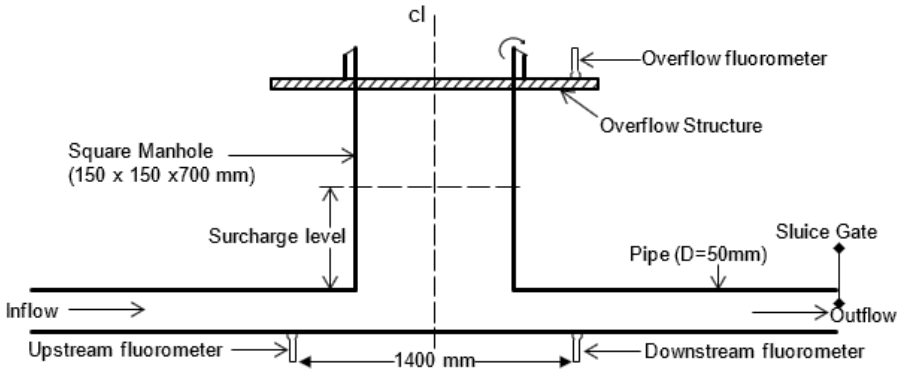

Figure 1: Schematic of the physical modelling setup

2.2 Tracer Measurement

Rhodamine Water Tracing dye with a maximum excitation wavelength of 555 nm and a maximum emission wavelength of 580 nm was used for the tracer measurement experiments. The neat Rhodamine WT dye is estimated to have a concentration of 10^9 parts per billion (ppb). For all the tests, diluted Rhodamine with a concentration of 1000 ppb (1 g/m^3) was continuously injected for 90 seconds and the tracer measurements continued for 15 minutes. Two overflow scenarios including one- and two-exits flow were investigated for a range of inflow discharge and Reynolds numbers. The first scenario models when the exit pipe becomes blocked and the only exit for the flow is via the top of the manhole. The second scenario is when there is an overflow in combination with a pipe exit. For each flow condition, the measurement was repeated five times to ensure the results derived from the tests are statistically significant. Bespoke computer algorithms were developed for automatic control of Rhodamine injection, tracer measurements, and flow conditions. The temporal variation of tracer

concentration was measured for fifteen minutes and at 30 Hz to capture high-resolution data on solute transport dynamics.

2.3 Instrumentation

The tracer study was conducted using peristaltic pump to provide controlled injection of the Rhodamine tracers. Two *313D* pump heads were fitted to the peristaltic pump to minimise pulsation and drew tracer from a 10-litre dye sump designed for this study. For each injection, depending on the experimental condition, a 5V signal with duration of 2-15 seconds, was sent to the peristaltic pump at a specified time using controller code. Three Turner Designs CYCLOPS-7 fluorometers were used to measure tracer concentrations within the system. All fluorometers were calibrated in-situ before conducting the tests to obtain the relationship between voltage readings and the change in concentration. Tracer measurements were conducted at the inlet pipe, the downstream end of the pipe and inside the overhead trough at the overflow to determine the evolution of tracer transport and dispersion. The upstream fluorometer was placed at 1850 mm from the injection point and 635 mm from the manhole entrance, the downstream fluorometer was installed at 1400 mm from the upstream fluorometer (see Fig. 1). The overflow fluorometer was positioned in a through where all the overflow water passes through (see Fig. 1). The overflow fluorometer was placed in a location to allow for mixing of the overflow content before reaching the measuring point and providing a fair representation of the overall pollutant concentrations in the overflow.

A flowmeter was installed to measure the incoming flow rate. The flowmeter comprises an electromagnetic Sitrans FM MAGFLO MAG 5100W and MAG 6000 transmitter. The flow within the system was manually calibrated to determine the actual flow in and out of the system, and the accuracy of the flowmeter during the experiment. The data from manual calibration show that the flowmeter was operating at 85% accuracy, with the actual output flowrate at 1.1723 times the input flowrate.

The flowrates tested in this study were selected to replicate a wide range of operational flows in sewer systems, considering the limitations of the laboratory setup. The discharge of 0.6 l/s was the lowest discharge that would create a full pipe condition in the manhole setup, while 1.4 l/s was the highest flowrate the experimental setup could accommodate when overflow conditions were created. The flow of 1.0 l/s represents the average between the possible minimum and maximum flowrates in the physical model. Input flowrates of 0.6 l/s, 1.0 l/s, and 1.4 l/s resulted in actual flowrates of 0.71 l/s, 1.17 l/s, and 1.64 l/s at steady-state condition, leading to the six output flowrates tested in this study. Table 1 summarizes the physical modelling conditions including the incoming flows, Reynolds, and velocity range. For the case of two-exit experiments, the incoming flow was split between the overflow and

downstream pipe outlet. It was observed that increase in the incoming flowrate had more influence on the flow discharge entering the overflow outlet in comparison to the downstream pipe.

Table 1: Summary of the hydrodynamic conditions tested within this study

	Pipe		Manhole (one exit flow)			Manhole (two exit flow)		
Incoming Q (m^3/s)	Uniform Velocity (m/s)	Reynolds number	Overflow Q (m^3/s)	Uniform Velocity (m/s)	Reynolds number	Overflow Q (m^3/s)	Uniform Velocity (m/s)	Reynolds number
0.00071	0.361	18000	0.00071	0.0316	4720	0.000216	0.0096	1440
0.00117	0.596	29700	0.00117	0.052	7770	0.000670	0.0298	4470
0.00164	0.835	41600	0.00164	0.0729	10900	0.001051	0.0467	7010

2.4 Data Analysis

The tracer data captured in voltage were converted to concentration using the equations derived from the fluorometer calibration tests. Using the Method of Moments (Equations 2-8), the characteristics of the tracer concentration profiles (i.e., the area, mass balance, variance and centroid arrival time) and the solute mixing behaviour were determined for all the test scenarios. The difference between the two measurements is taken as the mean travel time denoted by t_{50}.

The Method of Moments adopts the information of the area, centroid, and variance of the tracer concentration profile together with the frozen cloud approximation for the tracer distribution to convert between concentration-time and concentration-distance relationships, and determine the dispersion coefficient of the solute distribution (Cook et al., 2020; Jimoh, 2015; Rutherford, 1994).

The area, centroid and variance of a temporal concentration profile (m_0, m_1, m_2, respectively) for a series of discrete values are evaluated from the moments of the profile, defined by Equations 2 – 4:

$$m_0 = \Delta t \sum_{i=1}^{N} t_i^0 \, C_i \tag{2}$$

$$m_1 = \Delta t \sum_{i=1}^{N} t_i^1 \, C_i \tag{3}$$

$$m_2 = \Delta t \sum_{i=1}^{N} t_i^2 \, C_i \tag{4}$$

where Δt is the sampling interval (i.e. time step) of the data, C_i is the concentration of the i^{th} sample, t_i is the time at which the i^{th} sample was collected, and N is the total number of samples in the profile.

The centroid (μ) and variance (σ^2) of a concentration profile are calculated from its moments according to Equations 5 and 6, respectively:

$$\mu = \frac{m_1}{m_0} \tag{5}$$

$$\sigma^2 = \frac{m_2}{m_0} - \mu^2 \tag{6}$$

The dispersion coefficient is then determined following Equation 7:

$$D_{xx} = \frac{u^3}{2}\frac{\sigma_2^2 - \sigma_1^2}{x_2 - x_2} \tag{7}$$

where subscripts 1 and 2 refer to the upstream and downstream points, respectively, and the cross-sectional averaged velocity, u is calculated from the centroid of the profiles as:

$$u = \frac{x_2 - x_1}{\mu_2 - \mu_1} \tag{8}$$

A maximum entropy deconvolution algorithm (described by Equations 9 and 10) based on system theory was applied to the measure concentration profiles and identify the RTDs associated with urban drainage systems described by this study. The deconvolution method considers, the input/output relationship of the system in terms of a convolution integral between the upstream concentration and the RTD (Jimoh, 2015; Sonnenwald et al., 2015):

$$y(t) = \int_0^t x(t-\tau)E(\tau)d\tau \tag{9}$$

where $y(t)$ is the output i.e. overflow or downstream concentration, $x(t)$ denotes the input, i.e. upstream concentration, and $E(\tau)$ denotes the RTD. If $y(t)$ and $x(t)$ are measured, it is possible to deconvolve the unknown RTD, or in systems theory nomenclature, the impulse response.

To address the noise in the data and allow for regularisation, a single objective function is constructed using the Lagrangian equation as follows:

$$L(f, \lambda) = X^2(f) + \lambda S(f) \tag{10}$$

where (f) is the *N*-discretised estimate of the system response, the Lagrange multiplier (λ) a discriminator between the two functions, $X^2(f)$ denotes a weighted least squares distance metric between measured and simulated output, and $S(f)$ is the maximum entropy constraint function that encourages smoothness and positivity on the estimated response. Equations 9 and 10 were solved by an iterative process.

The predicted downstream trace from the deconvolution model described (Equations 9 and 10) was compared to the measured downstream trace using R_t^2 (Young, 1970) to provide a measure of the goodness of fit and evaluate the robustness of the deconvolution model to quantify dispersion and mixing processes in the square manhole. To obtain a unified comparison independent of the scale and specific flow conditions, the effects of the manhole volume was non-dimensioned using its normalised time defined as $t_{nz} = tQV^{-1}$, where t is the measured travel time, Q is the flowrate and V denotes the volume of fluid between two measuring points. The volume of fluid between the two measuring points was obtained by the summation of the volume of fluid in the pipe after the first fluorometer, the volume in the manhole, and the volume in the overflow trough before the second fluorometer (see Fig. 1). The normalised time (t_{nz}) was determined by dividing the measured time (t) by the nominal retention time (t_n). With the assumptions of presence of 'plug flow' condition and negligible effects from longitudinal dispersion, the nominal retention time, t_n within the fluid domain can be estimated from the ratio of the storage volume (V) to the flowrate (Q) as $t_n = V/Q$.

Following the analysis of the tracer data using the deconvolution algorithm, the results were compared to Taylor's advection-dispersion model described by Equation 1 to examine the model performance for quantifying the dispersion mechanisms and mixing patterns within the manhole. The longitudinal dispersion coefficient of the measured tracer data determined by the Method of Moments was compared to those obtained from the deconvolution model and the Taylors dispersion model to evaluate the appropriateness and robustness of these pollutant transport models for predicting mixing and dispersion for the case of the square manhole.

3.0 Results and Discussions

3.1 Hydraulic Characteristics and Concentration Distribution

Analysis of the incoming flow conditions shows that the manhole had laminar flow condition at an outflow of 0.216 x 10^{-3} m^3/s, and Re = 1440, while for all other flowrates turbulent flow conditions were established with Re ranging from 4470 to 10900.

Fig. 2 shows a sample of the temporal concentration profiles measured at upstream, downstream and overflow of the physical modelling setup. Due to the 90 seconds duration of dye injection, the upstream

tracer profile does not exhibit the Gaussian distribution expected for a pipe. However, the tracer profile measured at the upstream and downstream (within the pipe) is similar to the profiles obtained for a range of rectangular in-line storage tanks examined by Guymer et al. (2002). The overflow tracer measurements show a Gaussian distribution, with long tails recorded for all the tested conditions. Peak concentration values at the overflow are approximately 86-89% of the peak concentration at the upstream while the downstream peak is approximately 98-99% of the upstream peak concentration.

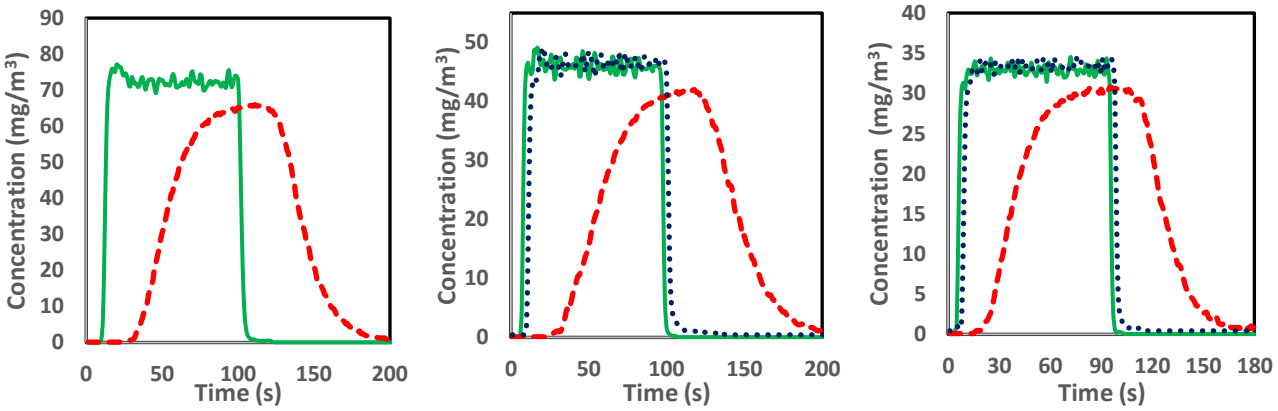

(a) 0.71 l/s for one-exit (b) 1.17 l/s for two-exits (c) 1.64 l/s for two-exits

Figure 2: Measured concentration profiles at upstream (green), downstream (black) and overflow (red)

The mass balance for the overflow tracer measurements was conducted and the results are shown in Table 2. For the test scenarios investigating 1-Exit flow, the recovery was between 93-100%, with slight deviations between trials. For the tests with a 2-Exit flow setup, the recovery of 92 to 101% was observed, with one outlier of 89% (see Table 2). The slight deviation from the 100% mass balance observed in the tracer data can be associated with the cut-off point applied to the data to avoid long tails of the tracer profiles.

Table 2: Mass balance between inflow and outflow concentrations

Inflow Q (m^3/s)	**0.00071**						**0.00117**						**0.00164**					
Trial No	1	2	3	4	5	Avg.	1	2	3	4	5	Avg.	1	2	3	4	5	Avg.
1-Exit (%)	93	94	96	95	94	94.4	95	96	95	94	96	95.2	95	94	100	95	99	96.6
2-Exit (%)	94	94	96	101	101	97.2	95	94	89	94	92	92.8	97	97	99	98	97	97.6

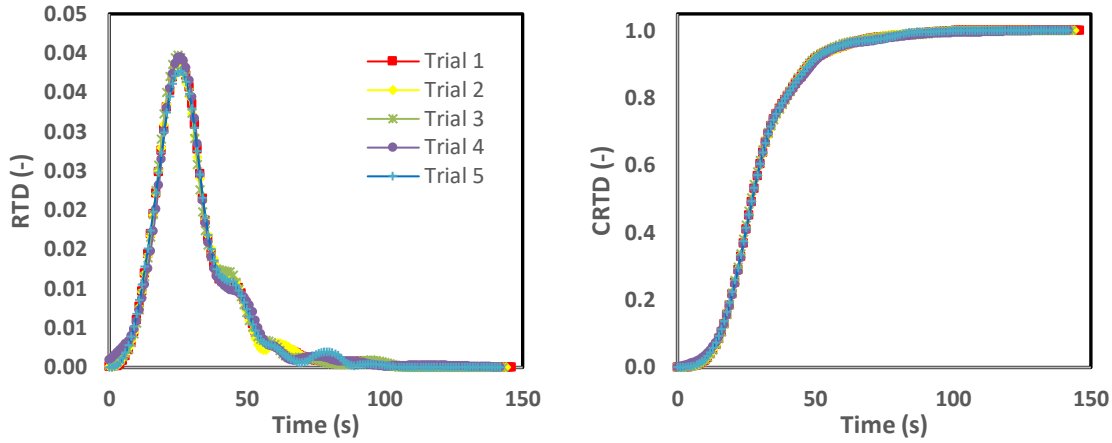

(a) One-exit overflow

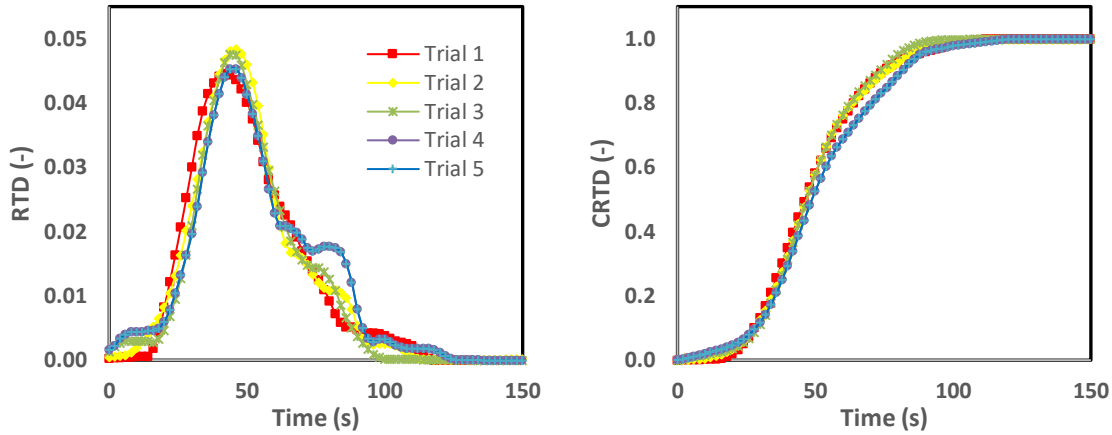

(b) Two-exits overflow

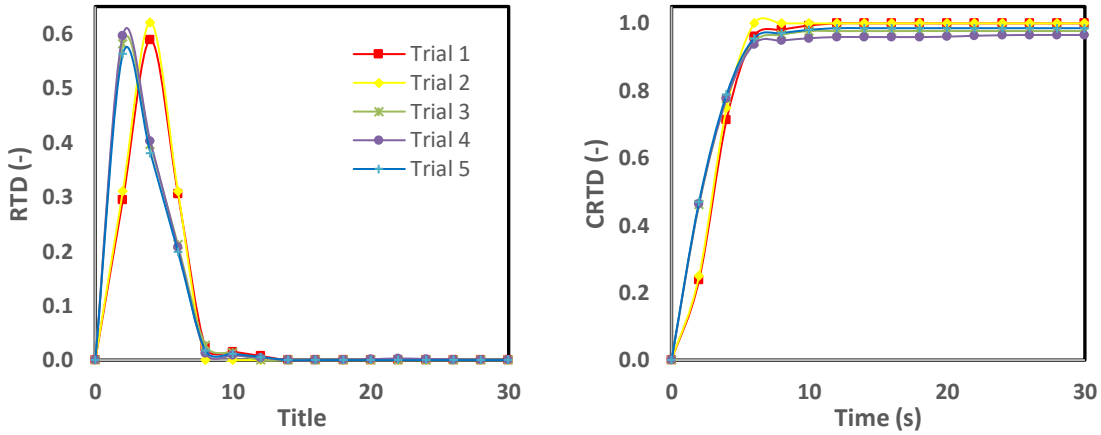

(c) Two-exits downstream

Figure 3: Deconvolved RTDs and CRTDs for the one- and two-exits scenarios at Q =1.17 l/s

3.2 Residence Time Distribution and Deconvolution Model

The Residence Time Distributions (RTD) and their corresponding Cumulative Residence Time Distributions (CRTD) for the overflow and downstream concentrations were obtained from the measured tracer data using the deconvolution method (Sonnenwald et al., 2015) described in §2.4. Figure 3 presents the RTDs and their corresponding CRTD curves determined from the tracer measurements for both one- and two-exit scenarios with a discharge of 1.17 l/s.

Figures 3a and 3b illustrate the temporal variation of tracer in the overflows for 1- and 2-exits flows. Both Figures show a Gaussian distribution of concentration profile which implies that a longitudinal dispersion mechanism is present in the square manhole. However, this is not the case for the downstream end (Figure 3c), where the RTD curves are similar to those of a typical surcharged manhole reported in previous studies (Guymer & Stovin, 2011; Jimoh, 2015). Although the same input flowrate of 1.17 l/s was tested for the two scenarios, the measured output flowrate was different between the one- and two-exits manhole setup. The shape of the overflow CRTD curves in both one-exit (Figure 3a) and two-exit (Figure 3b) scenarios suggests that the mixing characteristics in an overflowing manhole with turbulent flows are similar, irrespective of the output flowrate. For each of the five test repeats, mean CRTDs were generated by averaging all the individual CRTDs at the actual and normalised time for a specific test configuration (Figure 4).

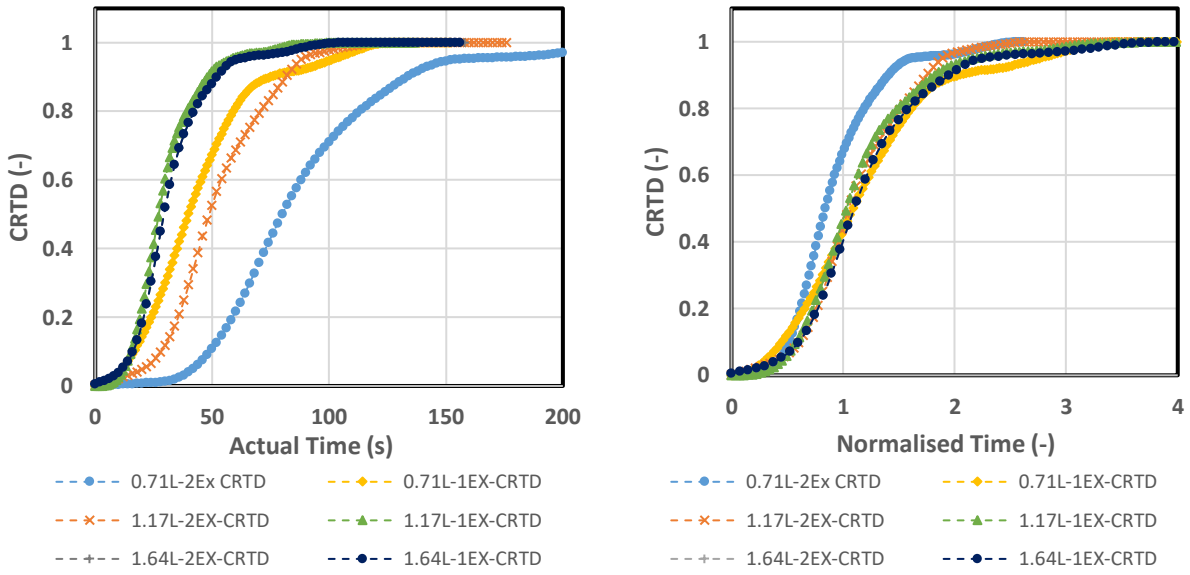

(a) CRTD at actual time (b) CRTD at normalised time

Figure 4: Compilation of CRTD curves for overflow manhole averaged at (a) actual time (b) normalised time

Figure 4 shows the mean CRTDs for both one- and two-exits overflows across all three flowrates investigated in this study. For the normalised time, all the CRTD curves collapsed into an individual curve which can be used as a representative curve showing the mixing characteristics occurring between the inlet and the overflow. The singular CRTD curve at the normalised time (Figure 4b) implies that the fluid, irrespective of the flowrate, has a similar retention time distribution. For laminar flow condition (i.e. 0.71 l/s, and 2-Exits scenario), the CRTD curve deviates from CRTDs of other flow conditions with a normalised t_{50} time of 0.84 in comparison to t_{50} of 1.1 for other flowrates.

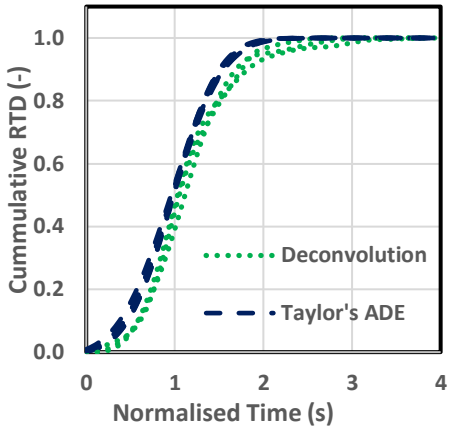

Figure 5: Comparison of overflow CRTDs determined from Deconvolution method with the Taylor's ADE Model.

3.3 Comparison of RTDs with Dispersion Models

Cumulative RTDs computed for the laboratory measurements using the deconvolution method are compared with Taylor's ADE model (Figure 5). The results from both deconvolution and ADE models have a cumulative profile, indicative that dispersion is occurring in the overflow. The dispersion coefficient values were obtained for the measured tracer profiles in the overflow using the method of moments, ADE, and deconvolution models. Table 3 compares the dispersion coefficients determined from different models examined in this study and presents new predictive formulae to determine mixing coefficients for square manholes across a range of flow conditions.

Table 3: Dispersion coefficients and statistical measures for method of moments, ADE, and Deconvolution methods

			Measured (Long tail)		Measured (Tail truncated)	Deconvolution		Optimised Taylor's ADE	
Q_{out} [m^3/s] $\times 10^{-3}$	Reynolds Number $\times 10^3$	Nominal Retention Time (s) $t_n = QV^{-1}$	Dispersion [m^2/s] $\times 10^{-3}$	Mean Residence Time t_{rtd} (s)	Dispersion [m^2/s] $\times 10^{-3}$	Dispersion [m^2/s] $\times 10^{-3}$	R^2	Dispersion [m^2/s] $\times 10^{-3}$	R^2
0.216	1.44	94.8	1.0	88.5	0.9	1.1	0.99	1.0	0.99
0.67	4.47	46.4	2.3	51.5	1.6	1.5	0.99	1.8	0.98
0.71	4.73	36.6	2.5	43.9	1.5	2.1	1.0	2.3	0.99
1.05	7.01	26.7	9.3	38.2	2.7	3.1	1.0	3.1	0.99
1.17	7.8	26.3	10.9	31.5	2.9	4.06	0.96	3.8	0.99
1.64	10.93	19.8	12.5	24.7	4.8	5.5	1.0	5.2	0.99
Predictive Relationships			$\mathbf{D_{xx}} = 7.55\boldsymbol{Q}$ (R^2 =0.9402) Eqn. 11		$\mathbf{D_{xx}} = 2.6672\boldsymbol{Q}$ (R^2 =0.9879) Eqn. 12	$\mathbf{D_{xx}} = 3.2073\boldsymbol{Q}$ (R^2 =0.9869) Eqn. 13		$\mathbf{D_{xx}} = 3.1302\boldsymbol{Q}$ (R^2 =0.9958) Eqn. 14	

For the measured concentration data, two dispersion coefficients were determined per-flow condition using the method of moments. The dispersion coefficients were determined based on the trace curves (distribution) using both long tails of the concentration readings, and the truncated tails at a point (time) where the concentration is approximately 0.05% of the peak measured concentration. Complex flow interactions and low-velocity tracer pockets within the manhole lead to long tails of low concentration tracer profiles which results in the overestimation of profile variance. The dispersion coefficients obtained from both long and truncated tails cases were then used to predict the overflow concentrations. Figure 6 compares the measured overflow concentrations with those obtained from non-ideal prediction models including the deconvolution and Taylor's ADE model. The analysis of the predicted data shows that both models can approximate the overflow concentration profiles for the square manhole with high precision. However, Taylor's ADE overestimated the peak overflow concentration by 7.4%, while the deconvolution model predicted the peak overflow concentration more robustly.

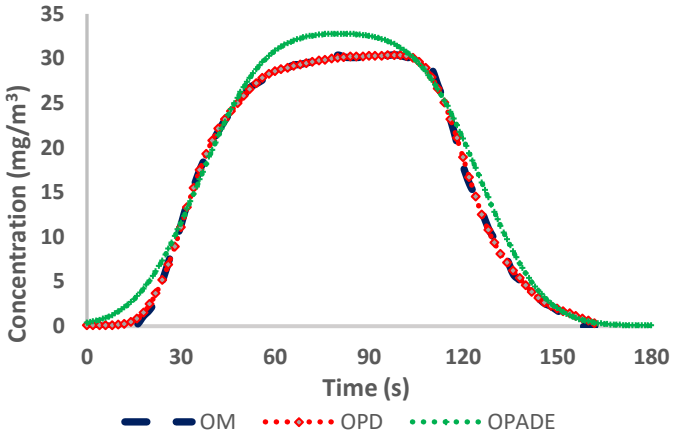

Figure 6: Comparison of measured and predicted overflow data [OM = Overflow measured, OPD = Overflow Predicted by Deconvolution, and OPADE = Overflow Predicted by Taylor's ADE]

4.0 Discussion

The RTDs determined using the deconvolution method (Figure 3) highlight the occurrence of mass flow oscillations at the outflow (Figure 3b). However, these oscillations were dampened with the increase in outflow rates (Figure 3a), indicative that the rates of dispersions are directly proportional to outflow rates. The analysis of the tracer concentration profiles shows that the deconvolution method can be robustly adopted to generate the RTDs from a step input upstream (Figure 3). In addition, the similarity between each trial curve gives credence to the accuracy and repeatability of the physical modelling results. The spread of the RTDs generated from the overflow data is however in multiples of the spread at the downstream pipe outlet (Figure 3c). The CRTD at the downstream ends shows formation of a jet flow, confirming the findings of Mark and Ilesanmi-Jimoh (2016), with a mean residence time approximately 10 times smaller than the one recorded at the overflow. Comparison of the CRTDs obtained from the deconvolution method for both 1-exit and 2-exits scenarios showed that for the measured time, CRTDs of 1-exit flow were almost identical, forming a single CRTD curve (Figure 4a). On the other hand, for the 2-exit flows, the curves exhibited a spread as the outflow rate reduces. The spread became less significant when the time was normalised by the volume, and all the CRTD curves except for that of laminar flow condition collapsed into one curve (Figure 4b). This singular curve can then be adopted as the descriptive curve for the mixing process occurring at the overflow.

Cumulative RTDs generated using Taylor's ADE model is plotted in Figure 5 and compared with those generated from the deconvolution method. Analysis of Figure 5 indicates that Taylor's CRTDs also collapsed into a single representative curve. The similarity between the CRTD curves determined from deconvolution method and Taylor's model indicates that both methods can comparatively describe the

underlying mixing processes occurring within the square manhole, and towards the overflow. Prediction of the overflow tracer and dispersion coefficient is determined using both models (Figure 6 and Table 3). Despite the overestimation of the peak concentrations by Taylor's model (Figure 6 and at the normalised time of 1.3-2 in Figure 5), the ADE model robustly predicted the overflow concentration with R^2 values above 0.98 (Table 3). This disparity is a common feature as Taylor's model tends to predict a higher peak concentration at the outlet due to idealised plug-flow assumption. The analysis of the dispersion results shows that prediction of the overflow concentrations from the deconvolution model had a better fit with the measured tracer data, and no overestimation of the peak concentration was observed.

Compatibility of the measured data with predictions from Taylor's ADE model suggests that the dispersion in the square manhole is greatly influenced by shear flow along the direction of flow, i.e. towards the overflow. In comparison to the four fundamental mixing regimes proposed by Danckwerts (1953), the CRTDs from this study suggests a "piston flow" condition with the occurrence of longitudinal mixing. The Piston flow with the occurrence of some longitudinal mixing signifies that the bulk of the tracer was being dispersed in the direction of the flow. The tracer's particles appear not to follow a back and forth or a random transport pathway. However, mixing occurred along the longitudinal direction due to the turbulence effects. The physical modelling results indicate that the mixing characteristics within an overflowing manhole with square geometry are less dependent on the flowrate once a turbulent flow regime is established (Figure 5b).

Comparison of the mean residence time (t_{rtd}) and the nominal retention time (t_n) for the 6 flow conditions tested within this study are presented in Table 3. For the outflow of 0.000216 m^3/s, the t_{rtd} value was less than the t_n, indicating the existence of dead zones within the square manhole. The measurements for the case of 0.000216 m^3/s show that the variance of the flow velocities is high, meaning that pockets of tracers are being trapped near the wall of the manhole. For the other overflows rates, i.e. turbulent flows, t_n was less than t_{rtd}, indicating that short-circuiting (bypassing) condition occurred. Short-circuiting condition implies that when a fully turbulent flow regime is developed, the tracers moved at a very fast speed and in a direct flow path towards the overflow, with minimal interactions with the manhole geometry (i.e., walls boundaries). For the three flow rates investigated in this study, the same normalised travel time (t_{nz}) of 1.2 ± 0.1 was obtained across both scenarios, except for the two-exits flow scenario at Q = 0.71 l/s where a slightly lower t_{nz} of 0.89 was achieved. A unified value of t_{nz} implies that if the manhole were to be replaced by an equivalent single pipe, the flow behaviour would tend towards those expected for the equivalent pipe. For the turbulent flows, the analysis indicates that the incoming flow spends a shorter reaction time between the manhole inlet and the overflow than the predicted retention time based on the manhole dimensions (i.e. predicted time =

1.2 times reaction time). On the other hand, the lower value of the normalised t_{nz} travel time, for the two-exits scenario with 0.71 l/s flowrate suggests that the incoming flow spends a longer reaction time than the predicted retention (i.e. predicted time =0.89 times reaction time).

4.1 Dispersion and Modelling

The dispersion coefficient is a robust measure to characterize solute transport and mixing processes in sewer systems. It represents the overall spreading of the solute residence time, often determined from measured tracer concentration data through the method of moments. The shortcoming of the method of moments for the determination of dispersion coefficient is its sensitivity to the smoothness of the concentration curve, as well as length of the distribution's tail. Using the full dataset (recordings over 300 seconds), predictive relationship between the measured tracer data and dispersion coefficient was derived as $\boldsymbol{D_{xx}} = 7.55\boldsymbol{Q}$ ($R^2 = 0.9402$). By applying a tail cut-off point equal to 0.05% of the peak concentration, the dispersion coefficient for the new distribution was determined as $\boldsymbol{D_{xx}} = 2.6672\boldsymbol{Q}$ ($R^2 = 0.9879$). A similar trend was reported by Bachmann and Tsotsas (2015), where the dispersion coefficient for the long tail data was twice that of the cut tail (short tail) data.

The D_{xx} computed from the deconvolution and Taylor's RTDs suggest dispersion coefficient to flowrate relationship of $\boldsymbol{D_{xx}} = 3.2073\boldsymbol{Q}$ ($R^2 =0.9866$) and $\boldsymbol{D_{xx}} = 3.1302\boldsymbol{Q}$ ($R^2 =0.9958$), respectively (see Table 3). The variation between predicted and measured dispersion coefficient values can go up to several orders, indicating that the dispersion coefficient in square manhole is not only a function of discharge. Other parameters such as the vertical variations of flow hydrodynamics over the depth, spatiotemporal variations of turbulence structure, geometrical properties of the sewer, and the sewer network design and operational conditions are also influencing the dispersion and mixing within the sewer and inside the manhole (Borzooei et al., 2020; Borzooei et al., 2019; Tenebe, Ogbiye, Omole, & Emenike, 2016; Wang & Chen, 2016). For the case of the square manhole configurations investigated in this study, the dispersion values from the predictive models were approximately 1.2 times higher than what was obtained from the method of moments with the cut tail. Using a 1-Dimensional ADE model, Romero-Gomez et al. (2009) obtained dispersion coefficients values in pipes, that are five times higher than those determined from the Method of moments. Although Romero-Gomez et al. (2009) study didn't provide the underlying reasons for the reported discrepancy between predicted and observed rates of axial dispersion, they suggested that experimental deviations from idealized mixing and flow condition (assumptions in ADE model) are likely to occur due to variation between the instantaneous and the time-averaged rate of dispersion.

The axial dispersion number, D_{xx}/UL, gives a non-dimensionalized quantification of the dispersion coefficient. When combined with the mean residence time, axial dispersion can be used to make predictions in different vessels. $D_{xx}/UL = 0$ indicates a perfect plug flow reactor, while a perfect continuous stirred tank reactor would have $D_{xx}/UL \rightarrow \infty$, $D_{xx}/UL = 0.025$ represents an intermediate amount of dispersion, and $D_{xx}/UL = 0.2$ denotes large dispersion values (Levenspiel, 1972). This study further determined the axial dispersion coefficients for all the measured tracer data and the three models examined in this study, i.e. method of moment, deconvolution and Taylor's ADE methods (Table 4). The results show the existence of an intermediate dispersion mechanism for all the overflow data. The values of the axial dispersion coefficient also indicate a diversion and transition from an ideal plug flow, however, yet not a completely mixed flow. This implies that whilst the flow moves towards the overflow as a jet, there is an element of back-mixing happening within the body of flow, although this mixing is limited. The flow is not instantly well-mixed and thus does not have the same concentration within different sections of the manhole.

Table 4: Axial dispersion coefficients

Q_{out} [m^3/s] $\times 10^{-3}$	Re	Measured (Long tail)	Measured (Tail Truncated)	Deconvolution	Optimised Taylor's ADE
0.000216	1440	0.084	0.071	0.0858	0.076
0.00067	4470	0.042	0.06	0.0705	0.080
0.00071	4730	0.046	0.062	0.0819	0.083
0.00105	7010	0.053	0.078	0.0958	0.095
0.00117	7800	0.053	0.078	0.1133	0.101
0.00164	10930	0.06	0.109	0.1252	0.111

Detailed analysis of the predictions provided from different dispersion models examined within this study shows that the D_{xx} obtained from the deconvolution method provide a more robust evaluation of overflow concentration when compared to the tracer data measurements. Hence, for the conditions tested within this study, the dispersion coefficient for square manhole can be described as Equation 13 (Table 3):

$$\mathbf{D_{xx}} = 3.2073\mathbf{Q} \tag{13}$$

A new dimensionless predictive relationship in terms of axial dispersion and Reynolds number is determined for the experimental data (Equation 15):

$$\frac{\mathbf{D_{xx}}}{\mathbf{UL}} = 8 \times 10^{-6} \times \mathbf{Re} + 0.0404 \quad (15)$$

The two predictive equations (Equations 13 and 15) proposed in this study can robustly model the hydraulic behaviour in the overflowing square manhole set-up investigated in this study. The proposed equations can also be adopted to predict dispersion coefficient and pollutant mixing in overflows from square manholes with similar configurations.

5.0 Conclusion

This paper investigates pollution transport and mixing processes in square manholes by undertaking physical and analytical modelling studies. The laboratory tests were designed to include a wide range of operational flows from laminar to fully turbulent flow conditions. Two pipe-manhole tests configurations of one and two-exits flow were investigated within the physical modelling study. Fluorometric tracer studies were conducted at the upstream, downstream, and within the manhole structure and overflow. RTD curves were determined from the tracer measurements using both deconvolution and Taylor's dispersion models. The dispersion coefficients were determined and the performance of different dispersion models examined in this study were evaluated using statistical error measures. The detailed analysis of the results shows that both deconvolution and Taylor's ADE models can reasonably approximate the overflow concentrations in square manholes. However, a comparison of the model's predictions with the physical modelling measurements shows that Taylor's ADE model overpredicted the peak overflow concentration. For the turbulent flow conditions, it was shown that RTDs can be described by a single representative curve at a normalised time. The tracer measurements highlighted the existence of a plug flow condition with an intermediate longitudinal dispersion.

At real-life scale, the physical model simulated in this study represents wastewater or flood water without any solid content. The peak overflow concentration at a similar manhole configuration would not be significantly reduced in comparison to the concentration at the inlet. Hence, when a sudden wastewater flush event is received at a manhole, the fluid particles within the flush would be transported towards the overflow. Most of the pollutant's particles would move solely in the direction of flow, although the effects of turbulence-induced dispersion can generate a limited amount of mixing. The tracer analysis highlights the formation of a dead zone within the manhole during laminar flow conditions, while short-circuiting was observed for the turbulent flow conditions tested in this study. The results indicates that upon occurrence of long-term laminar flow condition in the sewer-manhole

system, the continuous creation of dead zones can result in sedimentation and accretion of the pollutants within the square manhole. Similar configuration would be referred to as a poorly designed reactor in system engineering terminology. In such a reactor, if a completely mixed fluid is expected at the outlet, there would be a need to divide the total volume into multiple tanks (or reactors) arranged in series. In addition, if the flow through a similar configuration is laminar, dead zones would be created where pockets of the reactor volume would be inactive or released over an extended period of time. The proposed new predictive relationships derived for quantifying the dispersion coefficients can be incorporated into pollution transport models such as SWMM to describe solute transport and mixing for similar manhole geometries.

List of Symbols

Symbols	Parameter
Re	Reynolds number
R^2	
R_t^2	measure of the goodness of fit
D_{xx}	longitudinal dispersion coefficient [m^2/s]
D_{xx}/UL	axial dispersion number
c	concentration of tracer
A	the cross-sectional area of pipe [m^2]
M	mass of tracer [kg]
u	mean particle velocity derived from L/t_{rtd} [m/s]
t	Travel time
t_n	nominal retention time
t_{rtd}	mean residence time [s]
t_{nz}	normalised time
V	Volume of fluid
L	length between the input and output point [m]
Q	Flow rate [m^3/s]
μ	Centroid of concentration profile
σ^2	Variance of concentration profile

Acknowledgement

The authors would like to thank Ian Baylis for his technical support.

Reference

Abolfathi, S., & Pearson, J. (2014). SOLUTE DISPERSION IN THE NEARSHORE DUE TO OBLIQUE WAVES. *Coastal Engineering Proceedings*, *1*(34). doi:10.9753/icce.v34.waves.49

Abolfathi, S., & Pearson, J. (2017). APPLICATION OF SMOOTHED PARTICLE HYDRODYNAMICS (SPH) IN NEARSHORE MIXING: A COMPARISON TO LABORATORY DATA. *Coastal Engineering Proceedings*, *1*(35). doi:10.9753/icce.v35.currents.16

Bachmann, P., & Tsotsas, E. (2015). Analysis of Residence Time Distribution Data in Horizontal Fluidized Beds. *Procedia Engineering*, *102*, 790-798. doi:https://doi.org/10.1016/j.proeng.2015.01.190

Borzooei, S., Miranda, G. H. B., Abolfathi, S., Scibilia, G., Meucci, L., & Zanetti, M. C. (2020). Application of unsupervised learning and process simulation for energy optimization of a WWTP under various weather conditions. *Water Science and Technology*, *81*(8), 1541-1551. doi:10.2166/wst.2020.220

Borzooei, S., Teegavarapu, R., Abolfathi, S., Amerlinck, Y., Nopens, I., & Zanetti, M. C. (2019). *Impact Evaluation of Wet-Weather Events on Influent Flow and Loadings of a Water Resource Recovery Facility*, Cham.

Cook, S., Chan, H.-L., Abolfathi, S., Bending, G. D., Schäfer, H., & Pearson, J. M. (2020). Longitudinal dispersion of microplastics in aquatic flows using fluorometric techniques. *Water Research*, *170*, 115337. doi:https://doi.org/10.1016/j.watres.2019.115337

Danckwerts, P. V. (1953). Continuous flow systems: Distribution of residence times. *Chemical Engineering Science*, *2*(1), 1-13. doi:https://doi.org/10.1016/0009-2509(53)80001-1

Feng, B., Zhang, Y., & Bourke, R. (2021). Urbanization impacts on flood risks based on urban growth data and coupled flood models. *Natural Hazards*, *106*(1), 613-627. doi:10.1007/s11069-020-04480-0

GebreEgziabher, M., & Demissie, Y. (2020). Modeling Urban Flood Inundation and Recession Impacted by Manholes. *Water*, *12*(4), 1160. Retrieved from https://www.mdpi.com/2073-4441/12/4/1160

Goodarzi, D., Abolfathi, S., & Borzooei, S. (2020). Modelling solute transport in water disinfection systems: Effects of temperature gradient on the hydraulic and disinfection efficiency of serpentine chlorine contact tanks. *Journal of Water Process Engineering*, *37*, 101411. doi:https://doi.org/10.1016/j.jwpe.2020.101411

Guymer, I., Shepherd, W., Dearing, M., Dutton, R., & Saul, A. (2002). Solute Retention in Storage Tanks. In *Global Solutions for Urban Drainage* (pp. 1-11): American Society of Civil Engineers.

Guymer, I., & Stovin, V. R. (2011). One-Dimensional Mixing Model for Surcharged Manholes. *Journal of Hydraulic Engineering*, *137*(10), 1160-1172. doi:10.1061/(ASCE)HY.1943-7900.0000422

Jimoh, M. (2015). *Solute Mixing due to Square Manholes.* (PhD). University of Warwick, UK, Retrieved from http://wrap.warwick.ac.uk/77149/

Levenspiel, O. (1972). *Chemical reaction engineering*. New York: Wiley.

Mark, O., & Ilesanmi-Jimoh, M. (2017). An analytical model for solute mixing in surcharged manholes. *Urban Water Journal*, *14*(5), 443-451. doi:10.1080/1573062X.2016.1179335

Mark, O., Jørgensen, C., Hammond, M., Khan, D., Tjener, R., Erichsen, A., & Helwigh, B. (2018). A new methodology for modelling of health risk from urban flooding exemplified by cholera – case Dhaka, Bangladesh. *Journal of Flood Risk Management*, *11*(S1), S28-S42. doi:https://doi.org/10.1111/jfr3.12182

Miller, J. D., & Hutchins, M. (2017). The impacts of urbanisation and climate change on urban flooding and urban water quality: A review of the evidence concerning the United Kingdom.

Journal of Hydrology: Regional Studies, 12, 345-362. doi:https://doi.org/10.1016/j.ejrh.2017.06.006

Pham, B. T., Avand, M., Janizadeh, S., Phong, T. V., Al-Ansari, N., Ho, L. S., . . . Prakash, I. (2020). GIS Based Hybrid Computational Approaches for Flash Flood Susceptibility Assessment. *Water, 12*(3), 683. Retrieved from https://www.mdpi.com/2073-4441/12/3/683

Romero-Gomez, P., Li, Z., Choi, C. Y., Buchberger, S. G., Lansey, K. E., & Tzatchkov, V. T. (2009). Axial Dispersion in a Pressurized Pipe under Various Flow Conditions. In *Water Distribution Systems Analysis 2008* (pp. 1-10).

Rutherford, J. C. (1994). River mixing. Retrieved from http://catalog.hathitrust.org/api/volumes/oclc/28854092.html

Sañudo, E., Cea, L., & Puertas, J. (2020). Modelling Pluvial Flooding in Urban Areas Coupling the Models Iber and SWMM. *Water, 12*(9), 2647. Retrieved from https://www.mdpi.com/2073-4441/12/9/2647

Schreiber, C., Heinkel, S. B., Zacharias, N., Mertens, F. M., Christoffels, E., Gayer, U., . . . Kistemann, T. (2019). Infectious rain? Evaluation of human pathogen concentrations in stormwater in separate sewer systems. *Water Sci Technol, 80*(6), 1022-1030. doi:10.2166/wst.2019.340

Sonnenwald, F., Stovin, V., & Guymer, I. (2015). Deconvolving Smooth Residence Time Distributions from Raw Solute Transport Data. *Journal of Hydrologic Engineering, 20*(11), 04015022. doi:doi:10.1061/(ASCE)HE.1943-5584.0001190

Strohbach, M. W., Döring, A. O., Möck, M., Sedrez, M., Mumm, O., Schneider, A.-K., . . . Schröder, B. (2019). The "Hidden Urbanization": Trends of Impervious Surface in Low-Density Housing Developments and Resulting Impacts on the Water Balance. *Frontiers in Environmental Science, 7*(29). doi:10.3389/fenvs.2019.00029

Taylor, G. I. (1954). The dispersion of matter in turbulent flow through a pipe. *Proceedings of the Royal Society of London. Series A. Mathematical and Physical Sciences, 223*(1155), 446-468. doi:doi:10.1098/rspa.1954.0130

Tenebe, I. T., Ogbiye, A. S., Omole, D. O., & Emenike, P. C. (2016). Estimation of longitudinal dispersion co-efficient: A review. *Cogent Engineering, 3*(1), 1216244. doi:10.1080/23311916.2016.1216244

Von Sperling, M. (2007). *Wastewater Characteristics, Treatment and Disposalnull*: IWA Publishing.

Wang, P., & Chen, G. Q. (2016). Transverse concentration distribution in Taylor dispersion: Gill's method of series expansion supported by concentration moments. *International Journal of Heat and Mass Transfer, 95*, 131-141. doi:https://doi.org/10.1016/j.ijheatmasstransfer.2015.11.091

Water-UK. (2019). *Design and Construction Guidance for foul and surface water sewers offered for adoption under the Code for adoption agreements for water and sewerage companies operating wholly or mainly in England ("the Code")*. Retrieved from

Young, P. C. (1970). An instrumental variable method for real-time identification of a noisy process. *Automatica, 6*(2), 271–287. doi:10.1016/0005-1098(70)90098-1